Nuclear Materials and Energy 13 (2017) 28–34

Contents lists available at ScienceDirect

Nuclear Materials and Energy

journal homepage: www.elsevier.com/locate/nme

Chemisorption of a hydrogen adatom on metal doped α-Zr (0 0 0 1) surfaces in a vacuum and an implicit solvation environment

Cheng Zeng[a], Ben Wang[b,c], Lian Wang[b,c], Yingying Li[a,c], Yifan Nie[d], Wei Xiao[*,a,c]

[a] State Nuclear Power Research Institute, Beijing, 100029, PR China
[b] State Nuclear Bao Ti zirconium industry company, Baoji, 721013, P R China
[c] National Energy R & D Center of Nuclear Grade Zirconium Materials, Beijing, 100029, PR China
[d] Department of Materials Science & Engineering, the University of Texas at Dallas, Richardson, TX 75080, United States

ARTICLE INFO

Keywords:
Hydrogen adsorption
Zirconium
Transition metal
d-band model
Implicit solvation model

ABSTRACT

First-principles calculations have been carried out to investigate the adsorption of a hydrogen adatom on 24 metal doped α-Zr (0 0 0 1) surfaces in both a vacuum and an implicit solvation environment. The dopant are the elements in the 4th and 5th periods in the periodic table. Doping elements at the tail of the 4th and 5th periods can significantly reduce the hydrogen pickup in a vacuum environment. A weighted d-band center theory is used to analyze the doping effect. On the other hand, the hydrogen adsorption energies in water are relatively lower for all doped slabs and the surface adsorption of hydrogen adatom is stronger than that in a vacuum environment, especially, for the slabs with doping elements at the tail of the 4th and 5th periods. In the solvation environment, electronegativity difference affects the adsorption. Doping elements Ag, Ga, Ge, Sn, and Sb can reduce the hydrogen pickup in vacuum, while Ag and Cu can reduce the hydrogen pickup of the zirconium alloys in solvent environment.

1. Introduction

During the in-pile operation, the hydrogen is released by corrosion of zirconium alloys. Hydrogen degradation happens once the hydrogen generated by the corrosion is beyond the solubility in the substrate α-Zr [1]. Hydrogen degradation is important for the mechanical properties for the cladding materials in the nuclear power plants [1,2]. Numerous experimental studies have been carried out to evaluate the hydrogen pickup for material screening [3–5]. The hydrogen pickup fraction is defined as the ratio of the hydrogen adsorbed by the metal over the total amount of hydrogen generated during corrosion reaction [6]. It has been demonstrated that this parameter is closely related to the alloying elements, the type and proportion of intermetallic precipitates, microchemistry and the corrosion conditions [5,7,8]. For instance, although the concentration of certain alloying element is tiny, the hydrogen pickup can be lowered dramatically. For example, Ni is not good for hydrogen pickup because intermetallic precipitates form and they facilitate the hydrogen pickup [7]. In addition, it was documented that the hydrogen uptake fraction differs in different stages of the waterside corrosion [9]. Because passive oxide layer forms on the cladding, the oxidation layer may affect the hydrogen pickup. Doping elements in the oxidation layer may also affect the diffusion of the hydrogen atom [8,10]. During the stage of the oxidation layer growth, the compact passive film may crack and the zirconium alloy surfaces are exposed in the water. At this time, hydrogen adatom may be adsorbed on the zirconium surfaces [6].

Although experimental work can help engineer to design advanced zirconium alloys with a lower hydrogen pickup, a fundamental understanding of the interaction between the hydrogen adatom and the zirconium substrate is not clear. Without this knowledge, large amount of material screening experimental works are expensive and time consuming. Computational materials studies can help us investigate the material properties and optimize the material design process. For instance, the water adsorption and dissociation on transition metal doped zirconium surface, and the formation of various zirconium hydrides are well described using first-principles studies [11,12].

In this study, surface doping effects on hydrogen adsorption on α-Zr (0 0 0 1) surfaces are studied with first-principles calculations. The Zr (0 0 0 1) surface is doped with the elements in the 4th and 5th periods of the periodic table. The calculations are carried out in both a vacuum and an implicit solvation environment. The continuum solvation model is an effective method to simulate water environment. The interface of a Li_3OCl–cathode is studied with this model in solvation environment [13]. Moreover, this method is particularly useful in a heterogeneous

* Corresponding author.
E-mail addresses: xiaowei@snptc.com.cn, xiaowei1@gmail.com (W. Xiao).

http://dx.doi.org/10.1016/j.nme.2017.09.006
Received 8 June 2017; Received in revised form 24 September 2017; Accepted 25 September 2017
Available online 06 October 2017

electrochemical catalysis study, which mostly occurs in a solvated environment. For example, the oxidation of methanol on a Pt (111) surface, the oxygen evolution reaction on a IrO_2 (110) surface, the CO_2 electroreduction on a doped tin oxide surface, and perovskite $CH_2NH_3PbX_3$(X = Br, I) surface study [14–17].

2. Computational methods

2.1. Computational detail

The ground state energies of the adsorption systems are calculated with the density functional theory (DFT) calculations , which are performed with the Vienna ab initio simulation package (VASP) code [18]. The projected augmented wave (PAW) method is used to describe the wave functions near the core region [19]. The exchange correlation functional within the generalized gradient approximation (GGA) parameterized by Perdew, Burke, and Enzerof (PBE) is performed in our calculations [20]. The cutoff of the plane-wave kinetic energy is 400 eV. The integration over the Brillouin zone is performed using a 21 × 21 × 21 MonkhorstPack *k*-point mesh for the calculations of a zirconium unit cell, and a 3 × 3 × 1 *k*-point mesh for the slab calculations [21]. For the electronic relaxation calculations, the energy convergence criterion is 10^{-4} eV, where as in the ionic relaxations, the stopping criterion for the Hellmann–Feynman force minimization is 0.05 eV/Å. Spin polorization is used in all calculations, and all atoms are free to relax. The chemical adsorption energy of a hydrogen adatom on a metal atom doped zirconium (0 0 0 1) surfaces is defined as:

$$E_{ad} = E_{H/surf} - E_{surf} - \frac{1}{2}E_{H_2} \quad (1)$$

Here, $E_{H/surf}$ is the total energy of a zirconium slab with a hydrogen adatom on the (0 0 0 1) surface; E_{surf} is the system energy of a clean zirconium slab; and E_{H_2} is the energy of a hydrogen molecule. Charge transfer between the hydrogen adatom and the neighboring surface atoms is calculated, and the atomic partial charges are computed using the decomposition scheme proposed by Bader [22]. A 5 × 5 × 1 *k*-point mesh centered at Γ point and the Gaussian smearing method with the smearing width of 0.1 eV are used to calculate the density of state (DOS) of the doped zirconium surfaces.

The solvation effect is evaluated using an implicit solvation model developed by Mathew and Hennig [23,24] which is implemented into VASP code. The relative permittivity of water background is set as $\varepsilon_b = 80$ and the cutoff charge density is $\rho_{cut} = 0.0025$ Å^{-3}. The cavitation energies are calculated using a surface tension parameter of 0.525 meV/Å and the width of the dielectric cavity of 0.6 Å.

2.2. Computational models

The optimized lattice parameters of *α*-Zr are $a = 3.235$ Å, and $c = 5.159$ Å, which are close to the experiment data ($a = 3.231$ Å, $c = 5.148$ Å [25]). It also agrees with computational results calculated by Glazoff et al. well [26].

A super cell composed of 3 × 3 unit cells with six atomic layers of metal atoms is used to simulate the hydrogen adatom adsorption on a zirconium (0 0 0 1) surface. The surface energy converge test show that a six atomic layer slab is sufficiently to simulate surface adsorption. A vacuum layer on the top of the (0 0 0 1) surface is used to eliminate the interaction between the neighbor slabs since the periodic boundary condition is applied. The thickness of the vacuum layer is 15 Å. In order to study the hydrogen adsorption on an *α*-Zr (0 0 0 1) surface, a hydrogen adatom is located slightly above the surface (≈ 1.7 Å). Four possible adsorption sites are considered for a hydrogen adsorption process, the top site of a surface atom (top), the two-fold bridge site between two neighboring surface atoms (bri), the three-fold hcp and the fcc hollow sites around a surface atom (see Fig. 1). For the surface doping effect calculations, the central zirconium atom at the top atom layer of the super cell is substituted by a transition metal atom, which is in the 4th or 5th period of the periodic table.

To further validate the accuracy of the aforementioned parameters chosen in this work, the surface energy of an *α*-Zr (0 0 0 1) surface, and the binding energy and vibrational frequency of H_2 molecule are calculated. Without considering the zero-point energy, the surface energy is defined as:

$$E_{surf} = \frac{E_{surf} - E_{bulk}}{2A_{surf}} \quad (2)$$

where E_{surf} is the surface energy, E_{bulk} is the bulk energy of a bulk supercell with equivalent number of atoms, and A_{surf} is the surface area of the slab. The calculated surface energy of the zirconium (0 0 0 1) is 1.58 J/m^2, corresponding to 0.896 eV/atom, which agrees with both the experiments (0.80–1.05 eV/atom) and computational results (0.901 and 0.88 eV/atom) well [27–29]. The binding energy of a H_2 molecule is 4.55 eV, and the vibrational frequency is $\omega = 4269$ cm^{-1}, corresponding to a zero point energy of 0.266 eV. The results agree with experimental and computational data well [30,31].

3. Results and discussion

3.1. Hydrogen adatom adsorption on a Zr (0 0 0 1) surface in vacuum

3.1.1. Adsorption energies

The adsorption energies of a hydrogen adatom on transition metal doped Zr (0 0 0 1) surfaces in a vacuum environment are shown in Fig. 2. A hydrogen adatom is adsorbed on four possible adsorption sites of a Zr (0 0 0 1) surface. After relaxation, the hydrogen adatom may be repelled from the initial site and migrate to a second nearest neighbor site. For example, in the Fig. 3(a), the hydrogen adatom adsorbed on the Ag doped Zr (0 0 0 1) surface migrates to the second nearest neighbor hcp site after relaxation. Although after relaxation, the hydrogen adatom can stay on the top of the Ag atom, the adsorption energy is positive and it is not energetic favorable. This phenomenon has been reported by Nie et al. as well [12]. Although the adsorbed hydrogen adatom still stay around the doping defect, the surface distortion happens. For example, the adsorbed hydrogen pushes the Fe atom inward to the bulk, and the Fe moves close to the hydrogen adatom (see Fig. 3(b)) after relaxation. It indicates that the doping element of Fe shows high affinity towards the hydrogen adatom. The adsorption energies and the bond lengths of a hydrogen adatom on a Ag or Fe doped Zr slab in both vacuum and water environment are listed in the Table 1.

The hcp and the fcc hollow sites on a pristine Zr (0 0 0 1) surface are the energetically favorable sites for a hydrogen adatom, and the corresponding adsorption energies are − 0.99 eV at the fcc site and − 1.05 eV at the hcp site, respectively. The calculated results agree well with the values of − 0.96 eV and − 1.02 eV reported by Peng Zhang et al. [11]. On the other hand, the top site on a Zr (0 0 0 1) surface is the least stable adsorption position for a hydrogen adatom. Although the bridge position is also considered as an initial adsorption site, it is not a stable configuration. As a result, the adsorption energy of a hydrogen atom on the bridge site is not shown in Fig. 2. Suppose a hydrogen adatom is adsorbed on a doped zirconium slab in vacuum, a geometrical change happens after relaxation. In our calculations, the hydrogen adsorption does not change the configurations of the doped zirconium slabs too much and the hydrogen adatom is still around the initial position. The dopants of these slabs include V, Cr, Cu, Zn, Ga, Y, Zr, Nb, Mo, and Pd. In the second category, after relaxation the geometries of the slabs do not change significantly, but the hydrogen adatom can only stay on the top site or it migrates to second nearest neighbor site. The dopants of these slabs include Ge, Ag, Cd, In, Sn, and Sb. On the other hand, for Mn, Fe, Co, Ni, Ru, and Rh doped zirconium slabs, the surface distortion happens around the adsorption site near the doping elements.

Transition metal atoms are used to substitute a surface zirconium

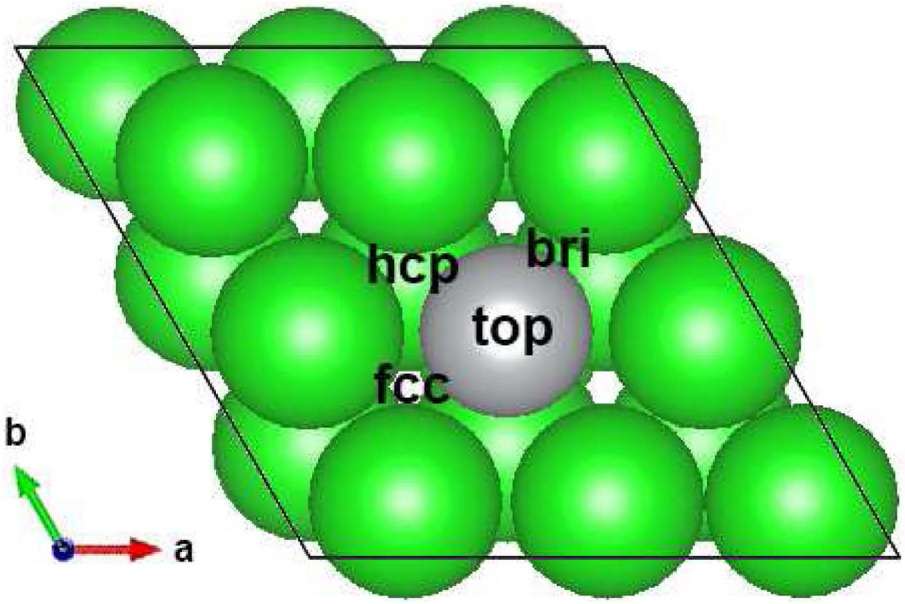

Fig. 1. Four possible adsorption sites for a hydrogen adatom on an α-Zr (0 0 0 1) surface.

atom. A hydrogen adatom is absorbed on the metal doped zirconium (0 0 0 1) surfaces around the doping atoms. For each surface doping system, the hydrogen adatom can be adsorbed around the doping surface atom at the four adsorption sites. All possible adsorption energies of a hydrogen adatom on doped Zr slabs in vacuum environment are listed in Table 2. The lowest adsorption energies for all of the doping system calculated in this work is represented by the royal blue solid line in Fig. 2. Technetium ($_{43}$Tc) is not considered in our calculation because of its high radioactivity. The adsorption energies of a hydrogen adatom on the doping surfaces at different adsorption sites are shown in Fig. 2 and it shows that the hcp or fcc sites are the most energetically favorable adsorption sites and the top one accounts for the least stable site for most of the doping elements in a vacuum environment. Periodical pattern appears for the adsorption energies of a hydrogen adatom on a doping surface with a 3d or a 4d transition metal doping element. For 4th and 5th period, the adsorption energy curves increase at the end of each period. It suggests that if those doping elements exist on the surface the adsorption of hydrogen is retarded on a zirconium (0 0 0 1) surface.

According to the magnitude of the adsorption energy, the doping elements can be divided into three categories. Consider the values of the adsorption energies, the three categories are: the adsorption of a hydrogen adatom is stronger than that on a pristine zirconium surface; the adsorption energies are close to that on a clean zirconium (0 0 0 1) surface; and the adsorption is weaker than that on a pristine zirconium surface. Evaluate the of the adsorption energies, the three group of doping elements are listed below:

- stronger than Zr: V, Fe;
- close to Zr: Sc, Ti, Co, Y, Nb, Mo, Cr, Mn, Ru, Rh, Pd, Ni, Cu, Zn;
- weaker than Zr: Ga, Ge, Ag, Cd, In, Sn, Sb

The doping effect of Sn, Ag, Nb, Cr, and Fe on the hydrogen adsorption on doped Zr (0 0 0 1) surfaces are investigated because these doping elements have already been used in the nuclear industry. Consider the adsorption energies, the sequence of the adsorption energies can be written as the order of Sn > Ag > Cr > Nb ≥ Zr > Fe. This result agrees with the experimental results well. Berry et al. studied binary zirconium alloy in which the dopant concentrations are less than 1.5 wt.%, and their results show that the dopants of Fe or Ni increase the hydrogen pick-up; on the contrary, Cr and Sb reduce the hydrogen pickup [32]. Couet et al. show that the hydrogen pickup

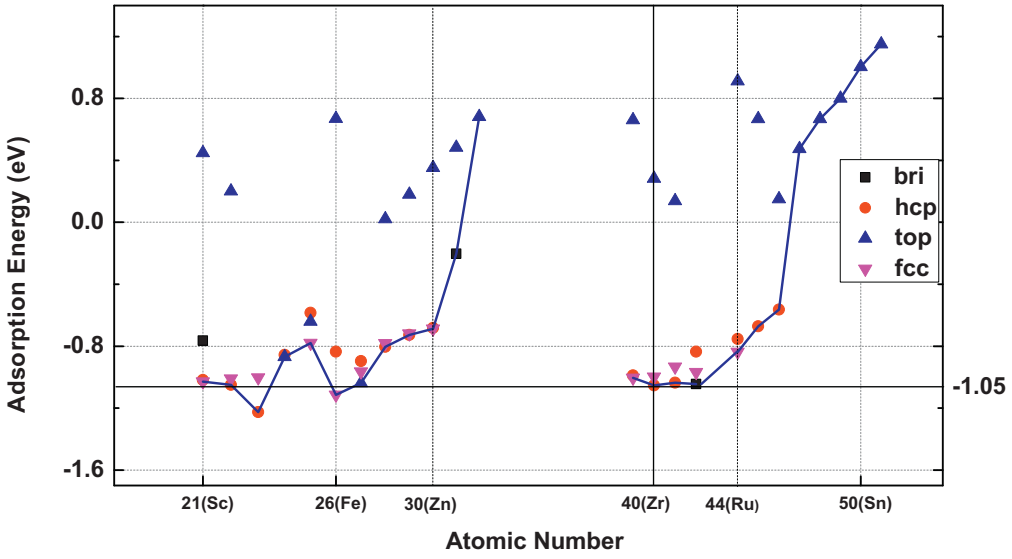

Fig. 2. Adsorption energies for a hydrogen adatom on Zr (0 0 0 1) surfaces at four different adsorption sites. Because some adsorption sites are not stable and the hydrogen adatom migrates to other position after relaxation, there are only one or two adsorption sites for certain doping system.

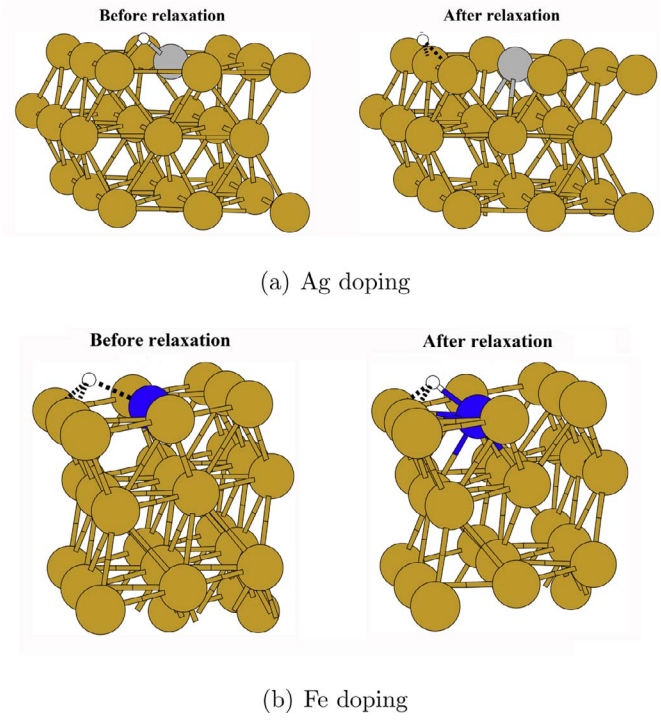

Fig. 3. Configurations of hydrogen adsorbed on a Ag (a) and Fe (b) doped Zr (0 0 0 1) surface before and after relaxation. Zr atoms are in yellow, the Ag atom is in gray, Fe atom is in blue, and the H adatom is in white. (For interpretation of the references to colour in this figure legend, the reader is referred to the web version of this article.)

Table 1
Adsorption energies of the doping systems with doping elements Ag and Fe in both vacuum and water environment. The bond lengths around the hydrogen atom are measured. M represents the doping element. 2 nn means the second nearest neighbor site.

	Ag				Fe		
	top	fcc	hcp	2 nn	top	fcc	hcp
E_{ad}@vac (eV)	0.47			− 1.04	0.67	− 1.11	− 0.84
Bond length M–H (Å)	1.70			–	1.82	1.72	1.80
Bond length Zr–H (Å)	–			2.14	–	2.16	2.12
E_{ad}@water (eV)	0.97		− 0.48		− 1.19	− 0.22	− 1.17
Bond length M–H (Å)	1.73		2.96		1.82	1.72	1.73
Bond length Zr–H (Å)	–		2.7		–	2.16	2.17

fraction is lowered in the zirconium alloy with 0.1–0.2 wt.% Cr or 1 wt.% Sn, while it increases in the alloy with 0.1–0.2 wt.% Fe or 0.5 wt.% Cu [6]. Choo *et. al* shows that the hydrogen uptake decreases slightly with the increase of the concentration of Nb (1 wt.%–20 wt.% Nb) [33]. It indicates that Sb, Cr, Sn, and Nb can reduce the hydrogen pick-up fraction, while Fe, Ni, and Cu increase it. In our case, the doping effects of Sb, Cr, Sn, Nb, and Fe agree with the experimental results. The doping effects of Ni and Cu does not agree with the experiments data. Since the doping element Ni forms precipitates of Zr_2(Fe,Ni), it may increase the hydrogen pickup [34]. The doping effect of Cu is not clear. For the real case, hydrogen pickup process is complicated and single element doping effect is not the only factor to affect this process. Moreover, the neutron adsorption cross section of doping elements Cd, In are very high, they can not be used in cladding materials. Our results indicate that except the neutron adsorbers, the doping elements which weaken the hydrogen adsorption can reduce the hydrogen pickup.

3.1.2. Electronic structure analysis: D-band model

A simple d-band model proposed by Hammer and Norskov can be used to analyze the hydrogen adsorption on transition metal doped zirconium surfaces [35–37]. As depicted in Fig. 4(b), the interaction between a hydrogen adatom and the metal surface can be considered as a two-step process. First, the H 1*s* electron interacts with the s and p bands of the surface metal atoms, and then a deep level filled with bonding state σ_g and an empty anti-bonding state σ_u^* are generated. The s–s or s–p coupling varies little for different transition metals. Therefore this attraction part does not change too much for different doping systems in this work. Second step, after the interaction of the first step, the H 1*s* electron interacts with the d-states and generates the bonding and anti-bonding states. The doping effect on hydrogen adsorption on a zirconium (0 0 0 1) surface is mainly determined by the contribution from d band electrons of the slab. Hammer et al. has shown that the interactions between the adsorbed molecules and the transition metal slabs are closely correlated to the d-band structure of the slabs. The d-band can be described by the average energy of the d-band of the surface metal atoms, called the d-band center. It is suggested that the lower d-band center is, the less active the surface becomes [38]. The d-band center of some doped slabs are calculated and its corresponding relationship with the hydrogen adsorption energy is analyzed.

Using the frozen potential approximation, the contribution of s–d band coupling to the adsorption energy of a hydrogen adatom can be written as [36]:

$$E_{\mathrm{d-hyb}} \sim -2(1-f)\frac{V^2}{\varepsilon_d - \varepsilon_{\mathrm{H}}} + \alpha V^2 \tag{3}$$

where ε_d is the center of d-band of slab, which is related with partial density of states of d-band electrons of the surface atoms bonded with the hydrogen adatom. ε_{H} is the center of s band of the hydrogen adatom, which is related with the partial density of states of H 1s. The idealized fractional filling factor f is the filling fraction of the d-bands of surface elements, which is approximately evaluated by $(v-1)/10$, where v is the valence electron numbers of the surface metal element [39]. For example, there are four valence electrons for Zr, as a result, $f = 0.3$. V refers to the coupling matrix between the hydrogen s orbital and the surface metal d state. α is a constant.

From the Eq. (3), metal elements with a full-filling d-band, for example, the elements at the end of the 4th and 5th periods, $1 - f = 0$, we only need to consider the αV^2 term. Therefore, the adsorption energies of a hydrogen adatom on noble metal doped surfaces are higher (the absolute values may be lower). On the other hand, for the doping elements with lower filling fraction, the adsorption energies decrease to more negative values and make the adsorption stronger [40]. That is why the zirconium surface is very active.

Although the d-band model can successfully describe the surface chemical reactivity of metallic for many studies [37], this model requires similar adsorption configurations for different metal slabs to evaluate their differences. In our study, the final adsorption sites for a hydrogen adatom on different doping Zr slabs may be different after relaxation. Since the coupling of the hydrogen 1*s* state to the d-band of the metal slabs is proportional to the s–d coupling matrix V (see Eq. (3)), it is reasonable to use the weighted d-band center to evaluate the chemical reactivity for a doping system. The weighted *d*-band center is obtained using the methods proposed in the previous pertinent works [41,42].

The adsorption energies E_{ad}, the calculated weighted d-band centers and the charge transfer to the hydrogen adatoms are calculated and listed in Table. 3. The charge transfer to the hydrogen adatom on the Sn (+ 0.28 |*e*|) or Ag (+ 0.21 |*e*|) doped Zr slab is much smaller than that of the other four doped Zr(0 0 0 1) slabs because the adatom is on the top site of the doping element, and the corresponding adsorption energy values of these two doping systems are high, or the adsorption is weak for these two doping systems. On the other hand, the weighted d-band center of Ag doped slab is much lower than that of the other four doping systems. As a result, the corresponding adsorption energy shows that the adsorption is weak. The weighted d-band centers of the Fe, Nb, and Cr doped slabs are relatively close to each other, since the hydrogen adatom sits in the three folder site for these cases and thus there are two

Table 2
Adsorption energies (eV) for hydrogen adsorption at four different sites on doped Zr (0 0 0 1) surfaces in vacuum. Dash line means that adsorption configuration is not stable and it becomes other configuration after relaxation.

Element	bri	hcp	top	fcc
21(Sc)	− 0.76	− 1.02	0.45	− 1.03
22(Ti)	–	− 1.05	0.2	− 1.01
23(V)	–	− 1.23	–	− 1
24(Cr)	–	− 0.86	− 0.87	–
25(Mn)	–	− 0.58	− 0.64	− 0.78
26(Fe)	–	− 0.84	0.67	− 1.11
27(Co)	–	− 0.9	− 1.04	− 0.96
28(Ni)	–	− 0.8	0.02	− 0.78
29(Cu)	–	− 0.73	0.18	− 0.72
30(Zn)	–	− 0.68	0.35	− 0.69
31(Ga)	− 0.2	–	0.48	–
32(Ge)	–	–	0.68	–
39(Y)	–	− 0.99	0.66	− 1
40(Zr)	–	− 1.05	0.28	− 1
41(Nb)	–	− 1.04	0.14	− 0.93
42(Mo)	− 1.05	− 0.84	–	− 0.97
44(Ru)	–	− 0.75	0.91	− 0.84
45(Rh)	–	− 0.67	0.67	–
46(Pd)	–	− 0.56	0.15	–
47(Ag)	–	–	0.47	–
48(Cd)	–	–	0.67	–
49(In)	–	–	0.8	–
50(Sn)	–	–	1	–
51(Sb)	–	–	1.15	–

zirconium atoms around the hydrogen adatom. The doping effect on the relation between the adsorption and the weighted d-band centers are not very clear. Because the adsorption site and the spin of certain magnetic element may also affect the weighted d-band center of a doping system [43]. For the noble metal doped systems with the same adsorption configuration, the lower the d-band center makes the surface less active in a vacuum environment.

3.2. Hydrogen adsorption on α-Zr (0 0 0 1) surfaces in an implicit water environment

3.2.1. Adsorption energies

Since the cladding tubes are in a water environment, it is interesting to simulate the hydrogen adsorption in water environment. A continuum solvation model is used in this work to lower the computationally costs because the simulation of an explicit solvent is very expensive. The adsorption energies of a hydrogen adatom on doped Zr (0 0 0 1) surfaces in a continuum solvation model are shown in Fig. 5.

All possible adsorption energies of a hydrogen adatom on doped Zr slabs with solvent are listed in Table. 4. Unlike the adsorption energies in a vacuum environment (see Fig. 2), the most stable adsorption sites for many doping elements are the top sites rather than the three-fold fcc or hcp sites. On the other hand, the adsorption energies in an implicit solvent background are lower than the counterparts in a vacuum environment. That is, a hydrogen adatom can be bonded more tightly on the zirconium alloy surfaces in a water environment, especially for the doping elements in the III A and IV A groups. For example, the adsorption energies of a hydrogen adatom on a zirconium slab doped with Cu and Ag in water environment are lower than that in vacuum environment for about 0.7 eV.

Table 3
The adsorption energies for a hydrogen adatom on transition metal doped Zr(0 0 0 1) surfaces, weighted d-band centers, and Bader charge transfer are calculated and listed in the table. Zr doping element is used for a pure metal reference.

Dopant	Fe	Zr	Nb	Cr	Ag	Sn
E_{ad} (eV)	− 1.11	− 1.05	− 1.03	− 0.87	+ 0.475	+ 1.0
ϵ_{d-w} (eV)	− 0.652	− 0.208	− 0.435	− 0.562	− 4.33	–
q_{vac} ($\|e\|$)	+ 0.55	+ 0.62	+ 0.62	+ 0.58	+ 0.21	+ 0.28

If a hydrogen adatom is adsorbed on a doped zirconium slab with solvent, a geometrical distortion may happen after relaxation. In our calculations, the hydrogen adsorption does not change the configurations of the doped zirconium slabs too much and the hydrogen adatom is still around the initial position. The dopants of these slabs include Cr, Fe, Co, Ni, Cu, Zn, Y, Zr, Nb, Mo, Pd, Ag, and Cd. Although after relaxation the geometries of the slabs do not change significantly, the hydrogen adatom in certain doped zirconium slabs can only stay on the top site or it migrates to second nearest neighbor site. The dopants of these category of slabs include Ga, Ge, In, Sn, and Sb. On the other hand, for V, Mn, Ru, and Rh doped zirconium slabs, the surface distortion happens around the adsorption site near the doping elements.

3.2.2. Energy contribution of the implicit solvation model

For the slabs with doping elements Cr, Nb, and Sn, the adsorption energies of a hydrogen adatom on the slabs can be written in a decreasing order of Zr > Sn > Nb > Cr. The results of hydrogen adsorption on Ag and Fe doped slabs are not considered here because their adsorption configurations in the vacuum and solvation environment are different. The adsorption energy differences between in an implicit solvation environment and the counterparts in a vacuum environment can be written as:

$$E_{\text{diel,sol}} = E_{\text{ad,sol}} - E_{\text{ad,vac}} \quad (4)$$

Here, $E_{ad,sol}$ is the adsorption energy in a water environment, and $E_{ad,vac}$ is the adsorption energy in a vacuum environment. The absolute values of the solvation energy contributions are in an increasing order of Nb ≤ Zr < Cr < Sn. It is reported that the energy variation due to the water background increases when the surface exhibits a partially ionic bond [24]. The ionic character between two elements can be approximated using the electronegativity difference. Similarly, the electronegativity difference between the dopant and Zr may affect the solvation energy contributions in water environment for zirconium alloy.

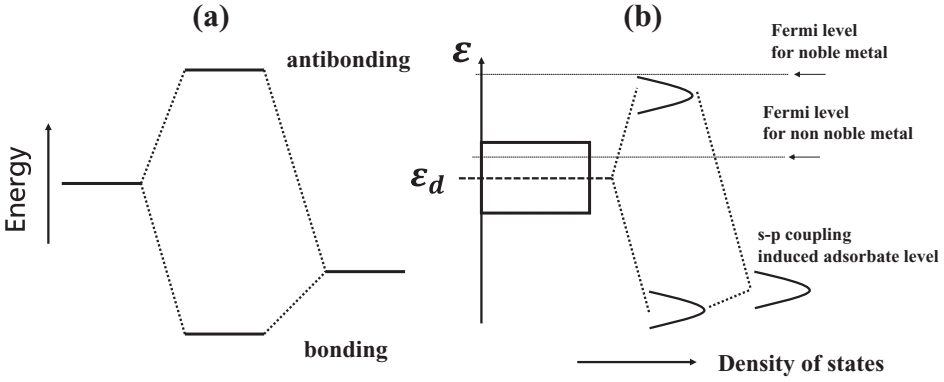

Fig. 4. Schematic illustration of the interaction between adsorbates and surface metals. (a) the simple case of two sharp atomic or molecule states. (b) the interaction of induced broadened adsorbate state with the *d* band of metal surface. ε_d refers to the center of d-band of the surface element [35].

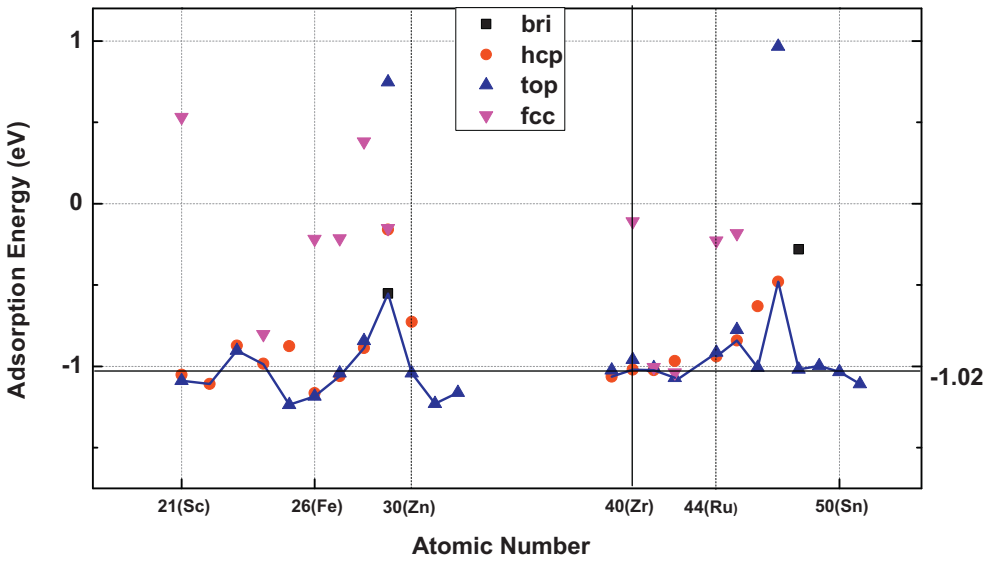

Fig. 5. Adsorption energies for an hydrogen adatom on doped (0 0 0 1) surfaces at different adsorption sites in a continuum solvation environment. Some adsorption sites are not stable in certain doping systems and they are not shown in this chart.

Table 4
Adsorption energies (eV) for hydrogen adsorption at four different sites on doped Zr (0 0 0 1) surfaces in a continuum solvation condition.

Element	bri	hcp	top	fcc
21(Sc)	–	−1.05	−1.09	0.53
22(Ti)	–	−1.11	–	–
23(V)	–	−0.87	−0.9	3.68
24(Cr)	–	−0.98	2.26	−0.8
25(Mn)	–	− 0.88	− 1.24	–
26(Fe)	–	− 1.17	− 1.19	− 0.22
27(Co)	–	− 1.06	− 1.04	− 0.21
28(Ni)	–	− 0.89	− 0.84	0.38
29(Cu)	− 0.55	− 0.16	0.75	− 0.15
30(Zn)	–	− 0.73	− 1.04	–
31(Ga)	–	–	− 1.23	–
32(Ge)	–	–	− 1.16	–
39(Y)	–	− 1.06	− 1.02	–
40(Zr)	–	− 1.02	− 0.96	− 0.11
41(Nb)	–	4− 1.02	− 1.01	− 1.01
42(Mo)	–	− 0.97	− 1.07	− 1.04
44(Ru)	–	− 0.94	− 0.91	− 0.23
45(Rh)	–	− 0.84	− 0.78	− 0.18
46(Pd)	–	− 0.63	− 1.01	–
47(Ag)	–	− 0.48	0.97	–
48(Cd)	− 0.28	–	− 1.02	–
49(In)	–	–	− 1	–
50(Sn)	–	–	− 1.03	–
51(Sb)	–	–	− 1.11	–

Table 5
The electronegativity difference $\Delta\chi$ and the solvation contribution $E_{\text{diel,sol}}$.

Dopant	$\Delta\chi$	$E_{\text{diel,sol}}$ (eV)
Nb	0.27	+ 0.01
Zr	0.00	+ 0.03
Cr	0.33	− 0.12
Sn	0.63	− 2.04

Therefore, the solvation contribution can be roughly evaluated by the electronegativity difference between the dopant and Zr. The Pauling scale electronegativity difference between two elements can be defined as:

$$\Delta\chi = \chi_M - \chi_{Zr} \quad (5)$$

Here, χ_M and χ_{Zr} are the electronegativity of the doping element and zirconium respectively and $\Delta\chi$ is the electronegativity difference between them. The electronegativity difference $\Delta\chi$, and the solvation contribution $E_{\text{diel,sol}}$ are listed in Table. 5. Another observation is that large electronegativity difference makes the hydrogen adsorption stronger. This table shows that larger electronegativity difference makes the adsorption energy difference higher between water and vacuum environments.

4. Conclusions

Chemisorption of a hydrogen adatom on 24 transition metal doped zirconium (0 0 0 1) surfaces is investigated using first-principles calculations, which is in a vacuum or an implicit solvent environment. Doping elements at the tail of the 4th and 5th periods can significantly reduce the hydrogen pickup in a vacuum environment. A weighted d-band center theory is used to analyze the doping effect. In a vacuum environment, doping elements Ga, Ge, Ag, Sn, and Sb may reduce the hydrogen pickup significantly.

In an implicit solvation environment, the hydrogen adsorption energies are relatively lower for all doped slabs and the surface adsorption of hydrogen is stronger than that in a vacuum environment, especially, for the slabs with doping elements at the tail of the 4th and 5th periods. Meanwhile, the adsorption sites are the top sites of the doping elements. In the solvation environment, electronegativity difference affects the adsorption. Doping elements Ga, Ge, Sn, and Sb can reduce the hydrogen pickup in vacuum, while Ag and Cu can reduce the hydrogen pickup of the zirconium alloys in solvent environment.

Acknowledgments

The authors acknowledge National Science and Technology Major Project of China under Contract No. 2015ZX06004001-002 and International Science and Technology Cooperation Program of China under Contract No. 2014DFA50800.

References

[1] V. Panasyuk, Hydrogen degradation of materials under long-term operation of technological equipment, Int. J. Hydrogen Energy 25 (1) (2000) 67–74, http://dx.doi.org/10.1016/S0360-3199(99)00006-3.
[2] V. Shestakov, A. Pisarev, V. Sobolev, S. Kulsartov, I. Tazhibaeva, Gas driven deuterium permeation through f82h martensitic steel, J. Nuclear Mater. 307–311 (2002) 1494–1497, http://dx.doi.org/10.1016/S0022-3115(02)01129-7.
[3] B.-Y. Kim, C.-J. Park, H.-S. Kwon, Effect of niobium on the electronic properties of passive films on zirconium alloys, J. Electroanal. Chem. 576 (2) (2005) 269–276, http://dx.doi.org/10.1016/j.jelechem.2004.11.002.
[4] A. Couet, A.T. Motta, B. de Gabory, Z. Cai, Microbeam x-ray absorption near-edge

spectroscopy study of the oxidation of Fe and Nb in zirconium alloy oxide layers, J. Nucl. Mater. 452 (1) (2014) 614–627, http://dx.doi.org/10.1016/j.jnucmat.2014.05.047.
[5] S. Kass, Hydrogen pickup in various zirconium alloys during corrosion exposure in high-temperature water and steam, J. Electrochem. Soc. 107 (7) (1960) 594–597, http://dx.doi.org/10.1149/1.2427781.
[6] A. Couet, A.T. Motta, R.J. Comstock, Hydrogen pickup measurements in zirconium alloys: relation to oxidation kinetics, J. Nuclear Mater. 451 (1) (2014) 1–13, http://dx.doi.org/10.1016/j.jnucmat.2014.03.001.
[7] B. Cox, Some thoughts on the mechanisms of in-reactor corrosion of zirconium alloys, J. Nucl. Mater. 336 (2) (2005) 331–368, http://dx.doi.org/10.1016/j.jnucmat.2004.09.029.
[8] INTERNATIONAL ATOMIC ENERGY AGENCY, Corrosion of Zirconium Alloys in Nuclear Power Plants, International Atomic Energy Agency, Vienna, 1992. IAEA-TECDOC-684
[9] M. Harada, R. Wakamatsu, The effect of hydrogen on the transition behavior of the corrosion rate of zirconium alloys, J. ASTM Int. 5 (3) (2008) 1–17, http://dx.doi.org/10.1520/JAI101117.
[10] C. Zeng, Y. Ling, Y. Bai, R. Zhang, X. Dai, Y. Chen, Hydrogen permeation characteristic of nanoscale passive films formed on different zirconium alloys, Int. J. Hydrogen Energy 41 (18) (2016) 7676–7690, http://dx.doi.org/10.1016/j.ijhydene.2016.01.174.
[11] P. Zhang, S. Wang, J. Zhao, C. He, Y. Zhao, P. Zhang, First-principles study of atomic hydrogen adsorption and initial hydrogenation of Zr(0 0 0 1) surface, J. Appl. Phys. 113 (1) (2013) 013706, http://dx.doi.org/10.1063/1.4772675.
[12] Y. Nie, W. Xiao, Chemical and physical adsorption of a H_2O molecule on a metal doped Zr (0 0 0 1) surface, J. Nuclear Mater. 452 (1) (2014) 493–499, http://dx.doi.org/10.1016/j.jnucmat.2014.05.066.
[13] S. Stegmaier, J. Voss, K. Reuter, A.C. Luntz, Li+ defects in a solid-state Li ion battery: theoretical insights with a Li_3OCl electrolyte, Chem.Mater. (2017), http://dx.doi.org/10.1021/acs.chemmater.7b00659.
[14] S. Sakong, A. Groß, Methanol oxidation on Pt(111) from first-principles in heterogeneous and electrocatalysis, Electrocatalysis (2017) 1–10, http://dx.doi.org/10.1007/s12678-017-0370-1.
[15] D.-Y. Kuo, J.K. Kawasaki, J.N. Nelson, J. Kloppenburg, G. Hautier, K.M. Shen, D.G. Schlom, J. Suntivich, Influence of surface adsorption on the oxygen evolution reaction on IrO_2 (110), J. Am. Chem. Soc. 139 (9) (2017) 3473–3479, http://dx.doi.org/10.1021/jacs.6b11932.
[16] K. Saravanan, Y. Basdogan, J. Dean, J.A. Keith, Computational investigation of CO_2 electroreduction on tin oxide and predictions of Ti, V, Nb and Zr dopants for improved catalysis, J. Mater. Chem. A (2017), http://dx.doi.org/10.1039/C7TA00405B.
[17] Y. Liu, K. Palotas, X. Yuan, T. Hou, H. Lin, Y. Li, S.-T. Lee, Atomistic origins of surface defects in $CH_3NH_3PbBr_3$ perovskite and their electronic structures, ACS Nano 11 (2) (2017) 2060–2065, http://dx.doi.org/10.1021/acsnano.6b08260.
[18] G. Kresse, J. Furthmller, Efficient iterative schemes for *ab initio*total-energy calculations using a plane-wave basis set, Phys. Rev. B 54 (16) (1996) 11169–11186, http://dx.doi.org/10.1103/PhysRevB.54.11169.
[19] G. Kresse, D. Joubert, From ultrasoft pseudopotentials to the projector augmented-wave method, Phys. Rev. B 59 (3) (1999) 1758–1775, http://dx.doi.org/10.1103/PhysRevB.59.1758.
[20] J.P. Perdew, K. Burke, M. Ernzerhof, Generalized gradient approximation made simple, Phys. Rev. Lett. 77 (18) (1996) 3865–3868, http://dx.doi.org/10.1103/PhysRevLett.77.3865.
[21] H.J. Monkhorst, J.D. Pack, Special points for Brillouin-zone integrations, Phys. Rev. B 13 (12) (1976) 5188–5192, http://dx.doi.org/10.1103/PhysRevB.13.5188.
[22] G. Henkelman, A. Arnaldsson, H. Jónsson, A fast and robust algorithm for bader decomposition of charge density, Comput. Mater. Sci. 36 (3) (2006) 354–360, http://dx.doi.org/10.1016/j.commatsci.2005.04.010.
[23] S. Sakong, M. Naderian, K. Mathew, R.G. Hennig, A. Groß, Density functional theory study of the electrochemical interface between a Pt electrode and an aqueous electrolyte using an implicit solvent method, J. Chem. Phys. 142 (23) (2015) 234107, http://dx.doi.org/10.1063/1.4922615.
[24] K. Mathew, R. Sundararaman, K. Letchworth-Weaver, T.A. Arias, R.G. Hennig, Implicit solvation model for density-functional study of nanocrystal surfaces and reaction pathways, J. Chem. Phys. 140 (8) (2014) 084106, http://dx.doi.org/10.1063/1.4865107.
[25] H. Xia, S.J. Duclos, A.L. Ruoff, Y.K. Vohra, New high-pressure phase transition in zirconium metal, Phys. Rev. Lett. 64 (2) (1990) 204–207, http://dx.doi.org/10.1103/PhysRevLett.64.204.
[26] M.V. Glazoff, A. Tokuhiro, S.N. Rashkeev, P. Sabharwall, Oxidation and hydrogen uptake in zirconium, zircaloy-2 and zircaloy-4: computational thermodynamics and ab initio calculations, J. Nuclear Mater. 444 (1) (2014) 65–75, http://dx.doi.org/10.1016/j.jnucmat.2013.09.038.
[27] Interfacial phenomena in metal and alloys, Physik in unserer Zeit 8 (1) (1977) 30–30, doi:10.1002/piuz.19770080108.
[28] X. Wang, M. Khafizov, I. Szlufarska, Effect of surface strain on oxygen adsorption on Zr (0 0 0 1) surface, J. Nuclear Mater. 445 (1) (2014) 1–6, http://dx.doi.org/10.1016/j.jnucmat.2013.10.046.
[29] G. Jomard, T. Petit, L. Magaud, A. Pasturel, First-principles investigation of the Zr (0 0 0 1) surface structure, Phys. Rev. B 60 (23) (1999) 15624–15627, http://dx.doi.org/10.1103/PhysRevB.60.15624.
[30] P. Zhang, S. Wang, J. Zhao, C. He, Y. Zhao, P. Zhang, First-principles study of atomic hydrogen adsorption and initial hydrogenation of Zr(0 0 0 1) surface, J. Appl. Phys. 113 (1) (2013) 013706, http://dx.doi.org/10.1063/1.4772675.
[31] P. Ferrin, S. Kandoi, A.U. Nilekar, M. Mavrikakis, Hydrogen adsorption, absorption and diffusion on and in transition metal surfaces: a DFT study, Surf. Sci. 606 (7) (2012) 679–689, http://dx.doi.org/10.1016/j.susc.2011.12.017.
[32] W.E. Berry, D.A. Vaughan, E.L. White, Hydrogen pickup during aqueous corrosion of zirconium alloys, Corrosion 17 (3) (1961) 109t–117t, http://dx.doi.org/10.5006/0010-9312-17.3.81.
[33] K.-N. Choo, S.-I. Pyun, Y.-S. Kim, Oxidation and hydrogen uptake of Zr based Nb alloys at 400C under 10 MPa H_2O steam atmosphere, J. Nuclear Mater. 226 (1) (1995) 9–14, http://dx.doi.org/10.1016/0022-3115(95)00115-8.
[34] A.T. Motta, A. Couet, R.J. Comstock, Corrosion of zirconium alloys used for nuclear fuel cladding, Annu. Rev. Mater. Res. 45 (1) (2015) 311–343, http://dx.doi.org/10.1146/annurev-matsci-070214-020951.
[35] B. Hammer, J.K. Nørskov, Why gold is the noblest of all the metals, Nature 376 (6537) (1995) 238–240, http://dx.doi.org/10.1038/376238a0.
[36] B. Hammer, J.K. Nørskov, Electronic factors determining the reactivity of metal surfaces, Surf. Sci. 343 (3) (1995) 211–220, http://dx.doi.org/10.1016/0039-6028(96)80007-0.
[37] J.K. Nørskov, T. Bligaard, J. Rossmeisl, C.H. Christensen, Towards the computational design of solid catalysts, Nat. Chem. 1 (1) (2009) 37–46, http://dx.doi.org/10.1038/nchem.121.
[38] J.R. Kitchin, J.K. Nørskov, M.A. Barteau, J.G. Chen, Modification of the surface electronic and chemical properties of Pt(111) by subsurface 3d transition metals, J. Chem. Phys. 120 (21) (2004) 10240–10246, http://dx.doi.org/10.1063/1.1737365.
[39] B. Hammer, Y. Morikawa, J.K. Nørskov, CO chemisorption at metal surfaces and overlayers, Phys. Rev. Lett. 76 (12) (1996) 2141–2144, http://dx.doi.org/10.1103/PhysRevLett.76.2141.
[40] B. Hammer, J.K. Nørskov, Theoretical surface science and catalysiscalculations and concepts, Advances in Catalysis, 45 Elsevier, 2000, pp. 71–129.
[41] V. Pallassana, M. Neurock, L.B. Hansen, J.K. Nørskov, First principles analysis of hydrogen chemisorption on PdRe alloyed overlayers and alloyed surfaces, J. Chem. Phys. 112 (12) (2000) 5435–5439, http://dx.doi.org/10.1063/1.481119.
[42] V. Pallassana, M. Neurock, L.B. Hansen, B. Hammer, J.K. Nørskov, Theoretical analysis of hydrogen chemisorption on Pd(111), Re(0 0 0 1) and Pd_{ml}/Re(0 0 0 1), Re_{ml}/Pd(111) pseudomorphic overlayers, Phys. Rev. B 60 (1999) 6146–6154, http://dx.doi.org/10.1103/PhysRevB.60.6146.
[43] S. Bhattacharjee, U.V. Waghmare, S.-C. Lee, An improved d-band model of the catalytic activity of magnetic transition metal surfaces, Scientific Reports 6 (2016) 35916, http://dx.doi.org/10.1038/srep35916.